ADVANCED MATERIALS
www.advmat.de

UV-Permeable 3D Li Anodes for In Situ Fabrication of Interface-Gapless Flexible Solid-State Lithium Metal Batteries

*Chuan Xie, Mingming Rong, Qianyi Guo, Zhenyao Wei, Zijian Chen, Qiyao Huang, and Zijian Zheng**

Flexible solid-state lithium metal batteries (SSLMBs) are highly desirable for future wearable electronics because of their high energy density and safety. However, flexible SSLMBs face serious challenges not only in regulating the Li plating/stripping behaviors but also in enabling the mechanical flexibility of the cell. Both challenges are largely associated with the interfacial gaps between the solid electrolytes and the electrodes. Here, a UV-permeable and flexible composited Li metal anode (UVp-Li), which possesses a unique light-penetrating interwoven structure similar to textiles is reported. UVp-Li allows one-step bonding of the cathode, anode, and solid electrolyte via an in situ UV-initiated polymerization method to achieve the gapless SSLMBs. The gapless structure not only effectively stabilizes the plating/stripping of Li metal during cycling, but also ensures the integrity of the cell during mechanical bending. UVp-Li symmetric cell presents a stable cycling over 1000 h at 0.5 mA cm^{-2}. $LiFePO_4$||UVp-Li full cells (areal capacity ranging from 0.5 to 3 mAh cm^{-2}) show outstanding capacity retention of over 84% after 500 charge/discharge cycles at room temperature. Large pouch cells using high-loading cathodes maintain stable electrochemical performance during 1000 times of dynamic bending.

1. Introduction

The rapid development of flexible and wearable electronics has posed an urgent need for advanced energy supply units in recent years. Desirable energy storage devices for flexible electronics shall possess adequate deformability, high energy density, stable cycling stability, and more importantly, high safety under abused mechanical deformation.[1–4] However, commercial lithium-ion batteries (LIBs) that are widely used in portable electronics can barely meet the aforementioned requirements: commercial LIBs are not flexible; their energy density is limited to 260 Wh kg^{-1}; the use of liquid electrolyte imposes intrinsic safety hazard.

Solid-state lithium metal batteries (SSLMBs) based on solid polymer electrolytes (SPEs) are one of the most promising solutions to reach high energy density and safety.[5–7] In comparison to the graphite anode used in LIBs, the Li metal anode is expected to bring remarkable gains in gravimetric and volumetric energy densities by ≈40% and ≈70%, respectively.[8–10] Solid electrolytes are known for their high safety because their high mechanical modulus can suppress the Li dendrites effectively and their high thermal tolerance can increase thermal runaway temperatures. SPEs are intrinsically lightweight and flexible so they are more suitable for flexible and wearable electronics than inorganic solid electrolytes.[11–14]

Despite the obvious advantages, there are still several critical challenges to address to achieve high-performance flexible SSLMBs. 1) Unlike the seamless liquid/solid interfaces between the liquid electrolyte and electrodes, there are serious concerns about the solid/solid interfacial gaps between the solid electrolyte and the electrodes.[15–17] These interfacial gaps significantly

C. Xie, Z. Zheng
Department of Applied Biology and Chemical Technology
Faculty of Science
The Hong Kong Polytechnic University
Hung Hom, Hong Kong SAR 999077, China
E-mail: tczzheng@polyu.edu.hk

The ORCID identification number(s) for the author(s) of this article can be found under https://doi.org/10.1002/adma.202406368

DOI: 10.1002/adma.202406368

M. Rong, Q. Guo, Z. Wei, Z. Chen, Q. Huang, Z. Zheng
School of Fashion and Textiles
The Hong Kong Polytechnic University
Hung Hom, Hong Kong SAR 999077, China

Q. Huang, Z. Zheng
Research Institute for Intelligent Wearable Systems
The Hong Kong Polytechnic University
Hung Hom, Hong Kong SAR 999077, China

Q. Huang, Z. Zheng
Research Institute for Smart Energy
The Hong Kong Polytechnic University
Hung Hom, Hong Kong SAR 999077, China

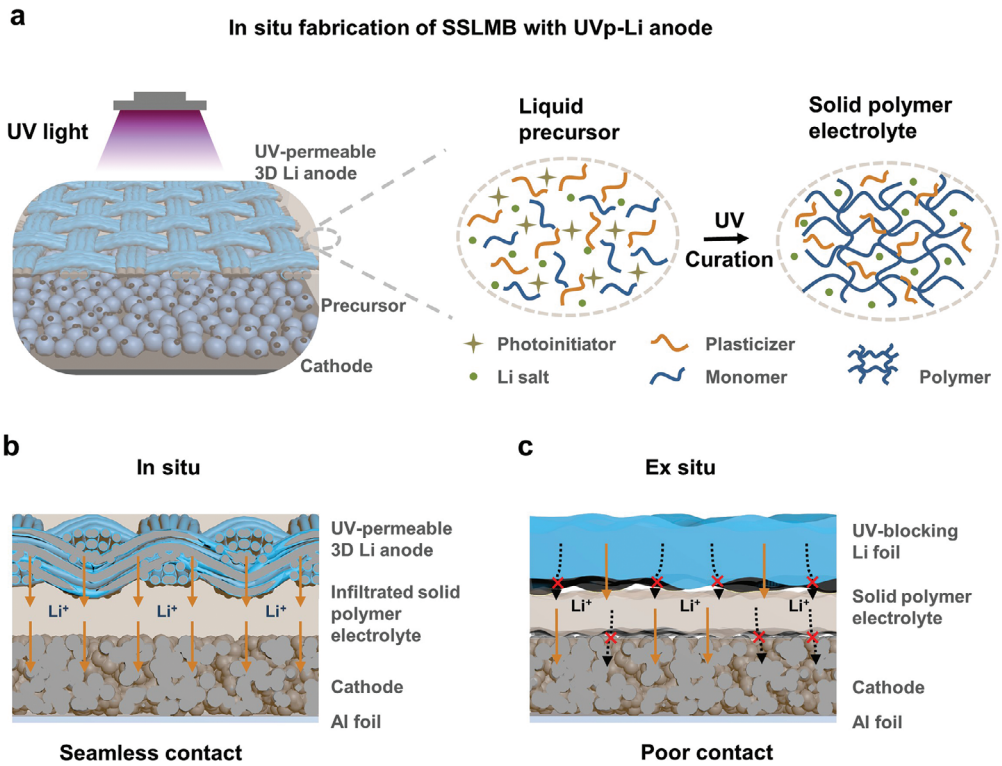

Figure 1. UV-enabled in situ fabrication of interface-gapless SSLMB based on UVp-Li. a) Schematic illustration showing in situ fabrication of SSLMBs and polymerization of liquid precursor under UV irradiation. b) Smooth Li^+ transport enabled by seamless interfaces of the in situ fabricated cell. c) Poor Li^+ transport due to the large gaps of the ex situ-assembled cell.

deteriorate the battery performance in terms of rate, capacity, and cycling stability. 2) The commonly used Li metal foil is not a flexible anode material. Therefore, it is also necessary to acquire a mechanically flexible and stable Li metal anode.[18,19]

To overcome the interface issue, researchers have developed the heat-induced in situ fabrication method, where liquid precursors of SPEs are filled into the preassembled dry cell and are subsequently polymerized by heating. By leveraging the flowable property of SPE precursors and heat-induced in situ polymerization,[20–24] the heat-induced in situ fabrication promotes seamless bonding of the solid electrolyte with both cathode and anode.[25–27] However, heat-induced polymerization usually takes a very long time (>24 h) for the complete conversion of monomers, resulting in the poor production efficiency for large-scale manufacturing. In addition, high temperature may induce the side reactions between Li metal and monomer/plasticizer, which may affect the energy performance of the battery cells.[28–30]

Alternatively, UV-induced polymerization is much faster than the heat-induced method; it only requires a few or a few tens of seconds to prepare the SPEs through fine-tuning of the monomers, the content of the photoinitiator, the light wavelength, and the intensity.[31–33] However, because battery electrodes are commonly light-blocking, the precursor solution of SPE is required to coat and cure on the surface of one electrode (either cathode or anode).[34–37] The other electrode is then postlaminated onto the opposite side of the polymerized SPE. As such, the UV-induced in situ polymerization can only ensure one gapless SPE/electrode interface, leaving the interfacial gaps on the other side unsolved. Some other methods that directly coat preformed SPEs onto the electrode surface via solution casting,[38–40] thermal infiltration,[41,42] and direct printing,[43,44] also result in similar interfacial gaps on at least one side of the electrode.

Herein, we report a UV-permeable composited Li metal anode (UVp-Li) that enables simultaneous UV-induced in situ polymerization of SPE with both cathode and anode, which leads to successful elimination of the interfacial gaps on both SPE/electrode interfaces. UVp-Li is made by compositing Li metal with conductive metal-coated carbon fiber fabric. The UVp-Li pertains to the 3D textile-like woven structure, which not only provides high flexibility to the electrode but also allows penetration of light through the interwoven holes. Therefore, UV-induced in situ polymerization can easily occur when the precursors are filled in between the cathode and anode, and shine UV light through the UVp-Li. Furthermore, the 3D composite enlarges the contact area between the UVp-Li anode and the SPE and decreases the local current density, leading to a remarkable cycling life of over 1000 h. $LiFePO_4$ (LFP)||UVp-Li full cell shows a high capacity retention of ≈84% after 500 cycles. We show that the UVp-Li is compatible with practical high areal capacity cathode (≈3 mAh cm^{-2}), and high-voltage cathodes such as $LiCoO_2$ (LCO), $LiNi_{0.6}Co_{0.2}Mn_{0.2}O_2$ (NCM622), and $LiNi_{0.8}Co_{0.15}Al_{0.05}O_2$ (NCA815). Flexible pouch cells over 10 cm^2 can be omnidirectionally bent over 1000 times without voltage fluctuation.

2. Results and Discussion

2.1. In Situ Fabrication of the SSLMBs with UV-Permeable 3D Li Anode

The key advantage of UVp-Li is that it enables in situ UV-initiated polymerization of SPE together with both cathode and anode. As shown in **Figure 1**a, the liquid precursor solution can easily infiltrate into the pores within the cell components and be readily turned into a solid state through UV-induced polymerization. The in situ fabrication of SSLMBs can eliminate the gaps at the interfaces (both the anode side and the cathode side) since the cured electrolyte provides continuous pathways for the migration of Li^+ within the whole battery (Figure 1b). In comparison, the construction of batteries in an ex situ way by stacking the cathode, solid electrolyte, and anode results in huge gaps at the interfaces and voids inside the electrodes, which prevents the smooth transfer of the Li^+ (Figure 1c). Besides, the 3D structure of the composited anode and the use of SPE can also benefit the stable plating/stripping of the Li metal during cycling which has been demonstrated to be an effective method by previous reports.[45–49]

The UVp-Li composite anode was fabricated by wicking the molten Li onto a metal-coated textile. In specific, a polymer-assisted metal deposition (PAMD) method[50,51] was first used to coat a thin layer of Cu on the surface of carbon cloth (Figure S1, Supporting Information). Then the molten Li metal rapidly wicked onto the Cu-coated fabric due to the high affinity of a trace amount of the surface Cu_2O (**Figure 2**a; and Figure S2, Supporting Information). Note that the loading amount of Li should be controlled so that the original pores on the fabric were not fully blocked (Figure 2b). The mass of the wicked Li metal was ≈2.8 mg cm^{-2}. The areal capacity of UVp-Li was determined to be ≈9.9 mAh cm^{-2}, matched well with the mass value considering the specific capacity of Li metal is 3680 mAh g^{-1} (Figure S3, Supporting Information). The light transmittance of UVp-Li was ≈3.1% for wavelengths ranging from 280 to 400 nm (Figure 2c). This transmittance is adequate for efficient UV-initiated polymerization. In contrast, Li foil would obstruct the light completely due to its light-blocking character and it showed almost 0% UV transmittance (Figure 2c,d).

To showcase the UV-permeable property, we shined UV light through the UVp-Li into a SPE precursor solution. We chose a plasticized SPE that could be readily polymerized when UV light was shinned onto its precursor solution containing Li salts, plasticizer, diacrylate monomer, photoinitiator 1173, and small portions of fluoroethylene carbonate (FEC) and lithium difluoro(oxalato)borate as additives (Figure 2e). A widely reported plastic crystal material, succinonitrile, was chosen as a plasticizer due to its high solvation ability with Li salts, good compatibility with acrylate-based polymers, and high antioxidation property at high voltage.[52–55] The UV light could penetrate through UVp-Li and lead to the polymerization of SPE precursor consequently (Figure 2f). The liquid precursor solidified quickly within 1 min of UV irradiation. In contrast, the UV light was fully blocked when the UVp-Li was replaced with conventional Li foil, and the liquid precursor remained in its liquid state without polymerization (Figure 2g).

The polymerized SPE was flexible and transparent (Figure 2h). It possessed a high electrochemical voltage window of up to 4.7 V under the linear sweep voltammetry (LSV) scan, indicating its potential in the application of high-voltage batteries (Figure 2i). The ionic conductivity of the plasticized SPE can be tuned through the change of the monomer ratio. A very high ionic conductivity of ≈1.02 mS cm^{-1} was obtained when the monomer ratio accounted for 20 wt% (Figure 2j), which was used for cell assembly. Note that the liquid FEC additive showed a slight influence on the ionic conductivity of SPEs with 20 wt% monomers at 25 °C (Figure S4a, Supporting Information). Besides, we also tested the ionic conductivity of SPE fabricated by the heat-induced polymerization method (Figure S4b, Supporting Information). It revealed that the SPEs show very close values of ionic conductivity regardless of the different polymerization methods. In addition to the high ionic conductivity, the obtained SPEs were nonflammable and could not be ignited when directly in contact with flame (Figure S5, Supporting Information).

2.2. Influence of In Situ and Ex Situ Fabrication on Interfacial Gaps

The electrochemical performances of solid-state batteries are directly influenced by the interfaces between the electrodes and the solid-state electrolyte. The UV-permeable property of UVp-Li not only enables facile UV-induced in situ fabrication of SSLMBs in an efficient way but also effectively avoids the formation of interfacial gaps. To prove the benefit of gapless interfaces through UV-induced in situ fabrication, three different types of symmetric cells, including "in situ-made," "single side-cured," and "ex situ-assembled" symmetric cells, were assembled and tested. To fabricate the in situ-made symmetric cell, a pair of UVp-Li with a 25 µm thick polyethylene separator in between were stacked and fixed by two clean glass slides. The SPE precursor solution was injected into the cell and then polymerized under 5 min of UV irradiation through the glass slides (**Figure 3**a). For the single side-cured symmetric cell, the SPE precursor solution was poured on one piece of UVp-Li and cured to form an SPE-infused UVp-Li. In the meanwhile, another set of SPE precursor solution was cured together with the polyethylene separator and the other UVp-Li under UV polymerization. The two pieces of pre-cured thin films were stacked together (Figure 3b). The ex situ-assembled cell was acquired by physically sandwiching the SPE-cured polyethylene separator with two pieces of pre-made SPE-infused UVp-Li (Figure 3c).

The morphologies and interfaces of the above-mentioned symmetric cells were examined by cross-sectional scanning electron microscope (SEM) imaging. For all samples, the 3D pores and interspace between the fibers and yarns of UVp-Li were filled with cured SPE, which significantly improves the interfacial contact areas between the electrode and the SPE and benefits quick Li^+ transfer within the electrodes (Figure S6, Supporting Information). Nevertheless, the interfaces of the symmetric cells present vastly different situations. Benefiting from the in situ UV curing of all cell components at once, no interfacial gap was observed in the in situ-made cell; both UVp-Li were tightly adhered to the SPE (Figure 3d). The single side-cured cell showed one gapless interface and one gapped interface (Figure 3e). In the ex situ-assembled cell, two poor interfaces with large voids and gaps were observed as the electrodes and SPE were only physically

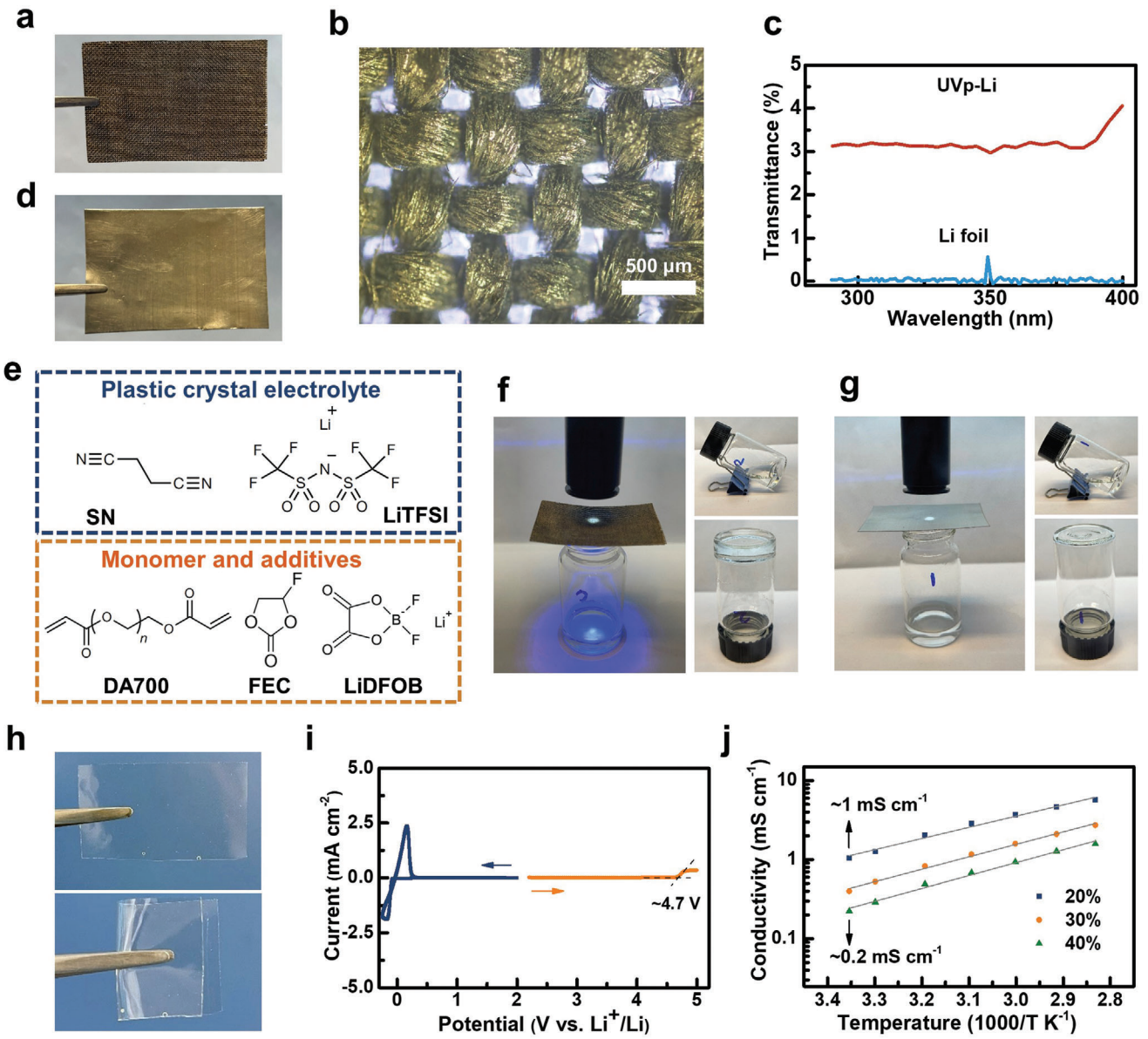

Figure 2. Fabrication and characterization of UVp-Li and SPE. a) Digital image of UVp-Li. b) Optical image showing the well-preserved porous structure of UVp-Li. c) UV transmittance of UVp-Li and Li anodes. d) Digital image of Li foil. e) Components of liquid precursor solution. f) Images showing that UV light penetrated through UVp-Li and the flowable liquid precursor was polymerized into SPE after 1 min irradiation. g) Images showing that Li foil blocked UV light and the liquid precursor maintained a flowable state even after 5 min irradiation. h) Optical images of the polymerized SPE in a flat and bent state. i) Electrochemical voltage window of the SPE. j) Ionic conductivity of the SPEs with different weight ratios of monomer.

contacted through external pressure without chemical bonding (Figure 3f).

The gapless interfaces offered a much-lowered impedance and overpotential when these electrochemical cells were tested. The interface differences of the symmetric cells can be reflected by electrochemical impedance spectroscopy (EIS). Upon assembly, the in situ-made cell displayed a bulk resistance (R_0) of ≈28 Ω and a charge transfer resistance (R_{ct}) of ≈132 Ω, which decreased slightly after 5 activation cycles (Figure 3g, blue solid and open squares). The fresh ex situ-assembled cell presented a large R_{ct} of ≈ 294 Ω and a large interfacial impedance (R_i) of ≈332 Ω based on the second semicircle at the middle-frequence region. After 5 activation cycles, the influence of interface can be minimized with R_i can be neglected while the R_{ct} also decreased significantly to ≈157 Ω (Figure 3g, green solid and open diamonds). The single side-cured cell exhibited similar behaviors as the ex situ-assembled cell but with lower R_{ct} and R_i (Figure 3g, red solid and open circles). The electrochemical stability of the symmetric cells was compared at room temperature under the same current density of 0.25 mA cm^{-2} and capacity of 0.5 mAh cm^{-2}. The in situ-made symmetric cell showed an overpotential of only ≈19 mV, lower than the single side-cured cell (≈34 mV) (Figure 3h). The ex situ-assembled cell displayed the highest overpotential of

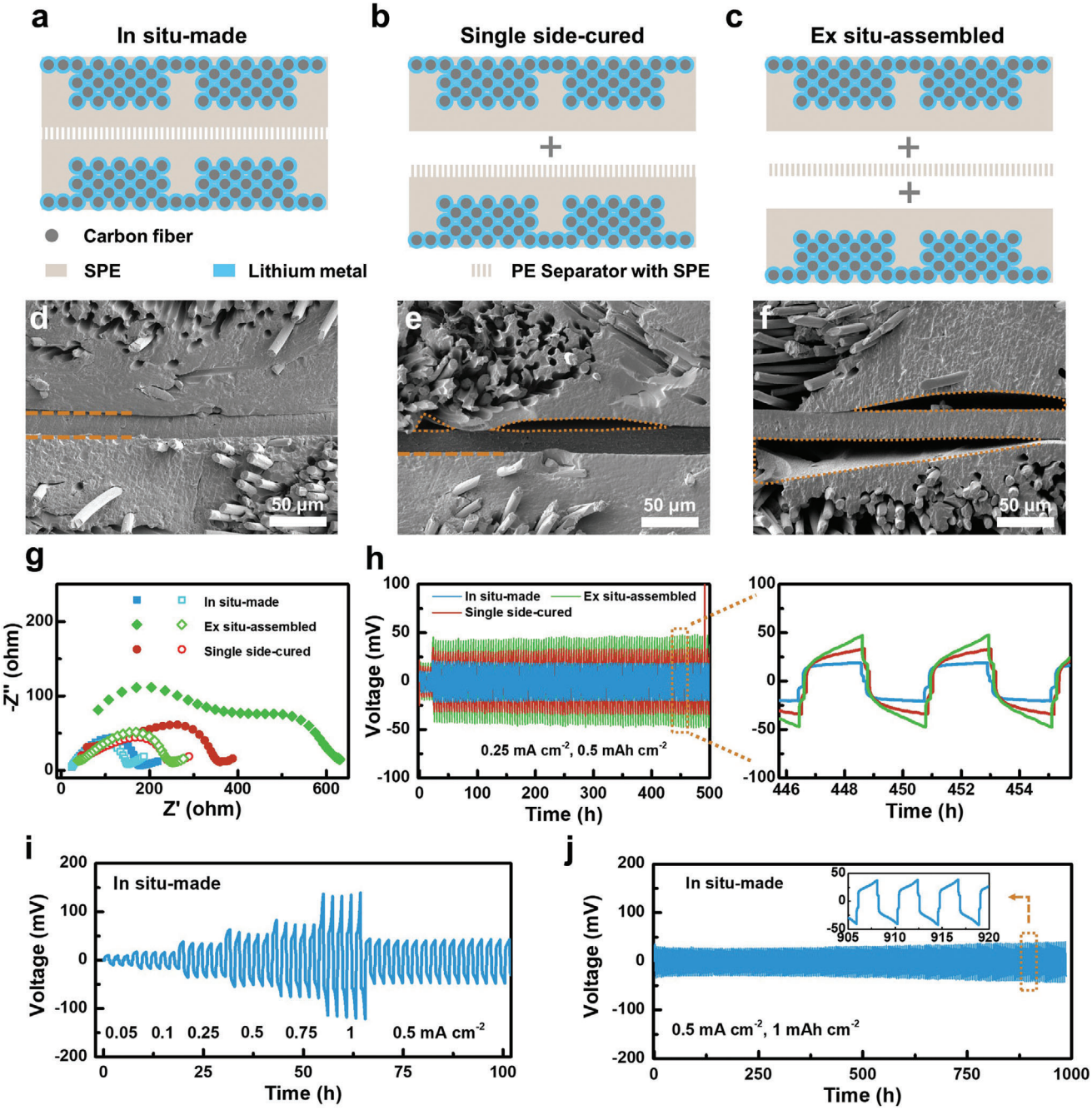

Figure 3. Influence of different fabrication methods on interfacial gaps and electrochemical performances. Schematic illustration of, a) in situ-made, b) single side-cured, and c) ex situ-assembled symmetric cells. Cross-sectional SEM images of, d) in situ-made, e) single side-cured, and f) ex situ-assembled symmetric cells. Please note that Cu-coated fabrics were used for SEM samples for the convenience of sample preparation. g) EIS results of symmetric cells before (solid symbol) and after (open symbol) 5 cycles of activation. h) Voltage profiles of the three symmetric cells. Inset, enlarged view of the voltage curves. i) Voltage of the in situ-made cell under different current densities. Each plating/stripping time was 2 h during cycling. j) Long-term cycling over 1000 h of the in situ-made cell at 0.5 mA cm^{-2} and 1 mAh cm^{-2}. Inset, enlarged view of the voltage curves.

≈47 mV because of the sluggish Li^+ migration at the two poor interfaces.

The intimate interfaces of in situ-made cells also enable high charge/discharge current densities. The overpotential of the cell increased gradually when the current density increased from 0.1 to 1 mA cm^{-2}, and the number only reached 105 mV when the current density was 1 mA cm^{-2}, exhibiting the advantages of the UV-induced in situ fabrication method and the 3D structure of the UVp-Li (Figure 3i). Long-term stability as high as 1000 h could be achieved for the in situ-made cell at a high current density of 0.5 mA cm^{-2} and capacity of 1 mAh cm^{-2} (Figure 3j). The overpotential remains below 50 mV even after long-time cycling (inset,

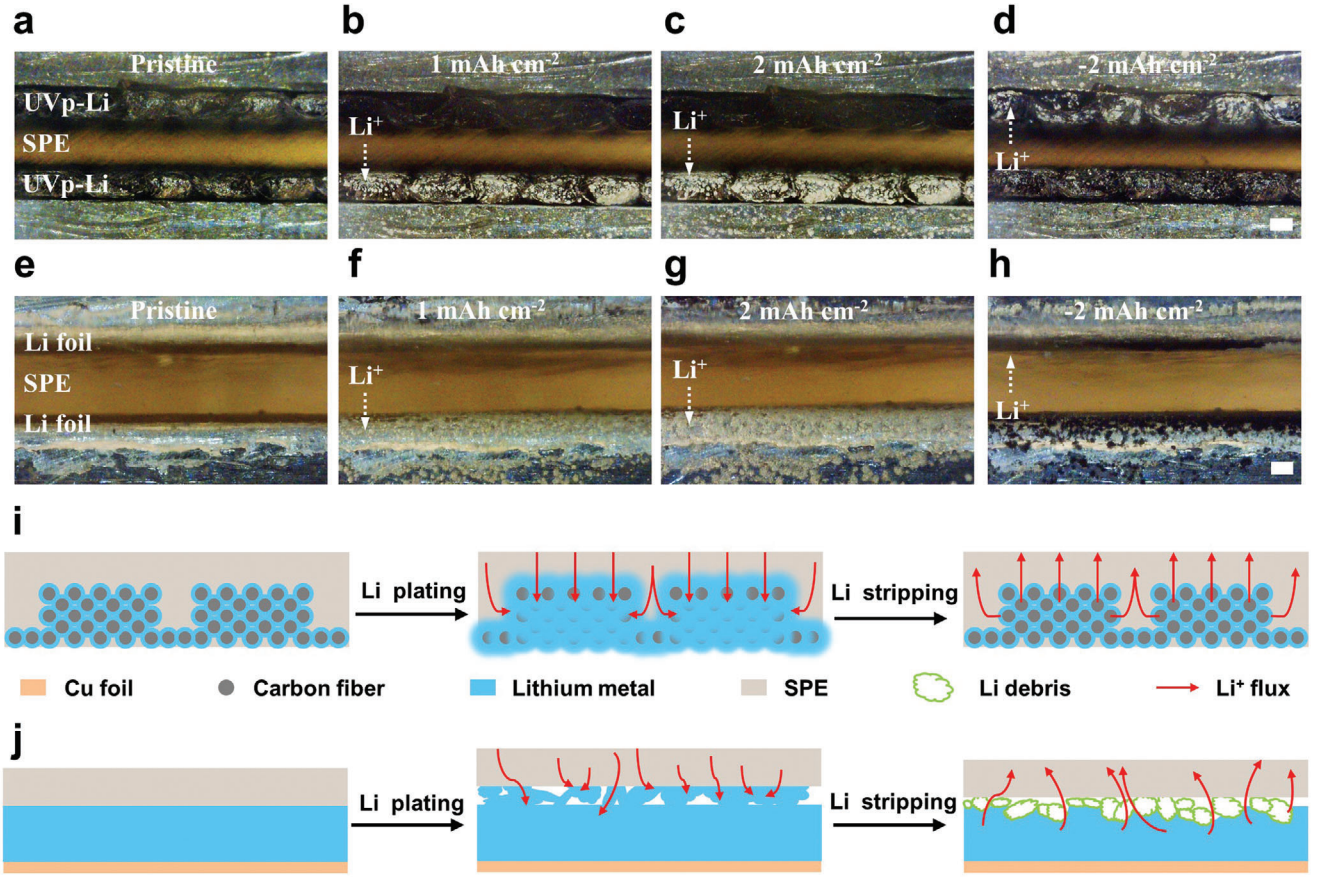

Figure 4. Li plating/stripping behaviors of UVp-Li and Li foil with SPE. a) Pristine symmetric UVp-Li||UVp-Li cell. Morphologies of UVp-Li after plating of, b) 1 mAh cm^{-2}, and c) 2 mAh cm^{-2} of Li. d) Morphologies of UVp-Li after stripping back of 2 mAh cm^{-2} Li metal. e) Pristine symmetric Li||Li cell. Morphologies of Li after plating of, f) 1 mAh cm^{-2}, and g) 2 mAh cm^{-2} of Li. h) Morphologies of Li after stripping back of 2 mAh cm^{-2} Li metal. The current density used for symmetric cells was 1 mA cm^{-2}. The scale bar is 100 μm in (a–h). Scheme showing the Li plating/stripping process of, i) UVp-Li, and j) Li foil.

Figure 3j). In contrast, the cells showing interfacial gaps could not be cycled at large current densities; the overpotentials quickly jumped to over 5000 mV when the current density was increased to 0.5 mA cm^{-2}.

2.3. Operando Study of Plating/Stripping Behaviors of UVp-Li

An operando optical study was carried out to explore the plating/stripping behaviors of UVp-Li using a homemade electrochemical setup with a transparent glass cover. Two electrodes of UVp-Li were separated by a polydimethylsiloxane spacer, and UV-induced in situ polymerization was applied to ensure good contact at interfaces after injection of the liquid precursor. Li was stripped from the upper UVp-Li and plated onto the bottom UVp-Li (**Figure** 4a). During the stripping period, the shiny color of the stripped UVp-Li (upper electrode) became darker. Li was plated throughout the entire 3D structure of the bottom UVp-Li without forming any dendrites (Figure 4b,c).[56–58] We then reversed the plating process from the bottom electrode to the upper one and observed a similar phenomenon (Figure 4d). The morphologies of the cycled UVp-Li were examined through SEM. The surface of the UVp-Li electrode was flat, with pores and inner space between yarns and fibers filled with SPE after preparation (Figure S7a, Supporting Information). The structure remained stable with voids and gaps appearing between the fibers after being stripped (Figure S7b, Supporting Information). After plating back of Li, the plated Li metal concentrated on the inner voids and gaps between conductive fibers instead of uniformly covering the whole surface, maintaining good contact at the intact SPE-filled area (Figure S7c, Supporting Information).

As a comparison, we also assembled similar cell using Li foils (Figure 4e). In the plating process from the upper Li foil to the bottom one, the surface of the plated Li foil became much rougher due to the nonuniform deposition of Li (Figure 4f,g). In the reversed deposition, a large number of dark particles were observed at the bottom Li foil, which are ascribed to Li debris consisting of dead Li and SEI (Figure 4h). The surface of Li metal was examined before and after the cycling process. Voids formed easily for stripped Li foil, leading to poor contact between the Li and SPE. Consequently, protuberances and dendritic structure formed after plating Li back, further deteriorating the interfaces (Figure S7d–f, Supporting Information).

The plating/stripping behaviors of UVp-Li and Li anode can be described by illustration schemes shown in Figure 4i,j, respectively. The 3D contact between the porous UVp-Li and SPE can promote the Li^+ migration and transfer within the electrode, and suppress the formation of dead Li. The plated Li can be efficiently deployed back to the counter electrode when the current is reversed. In contrast, because of the planar contact between the Li foil and SPE, the Li deposition on Li foil shows an inhomogeneous distribution. The plated Li cannot be fully deployed upon stripping; the accumulation of Li debris on the surface shall lead to an inferior performance of the battery.

2.4. Electrochemical Performance of SSLMBs Using UVp-Li

SSLMBs were assembled using LFP cathode and UVp-Li (or Li foil) anodes. By taking advantage of the UV-permeability of UVp-Li, the LFP||UVp-Li cell was fabricated through a UV-induced in situ fabrication method described above. The LFP||Li cell was prepared by curing the LFP cathode and separator together with SPE precursor under UV and subsequently laminating onto a commercial Li foil. Importantly, LFP||UVp-Li presented seamless interfaces at both UVp-Li|SPE and LFP|SPE sites. The pores within the LFP particles and the interspace of the UVp-Li were occupied by the UV-cured SPE (**Figure 5**a), guaranteeing the smooth transfer of Li^+ during cycling. LFP||Li, however, showed only one good interface at the LFP|SPE site, but large gaps at the Li|SPE site (Figure 5b). The poor interfacial contact leads to high interfacial resistance of the full cell. The difference in the interfacial resistance was verified by the EIS characterization. LFP||UVp-Li delivered much lower (≈120 Ω) resistance than LFP||Li (≈275 Ω) upon assembly (Figure 5c). The resistance of LFP||UVp-Li increased moderately to ≈170 Ω after cycling and stabilized gradually in the following cycles (Figure S8, Supporting Information), being still much smaller than that of LFP||Li after cycling (≈356 Ω).

LFP||UVp-Li showed much better capacity and cycling stability than LFP||Li. LFP||UVp-Li could deliver a specific capacity of ≈146, 137, 130, 120, 105, and 90 mAh g^{-1} at the C-rates of C/10, C/5, C/4, C/3, C/2, and 1 C, respectively, much higher than LFP||Li (Figure 5d). Due to the large interfacial resistance, the specific capacity of LFP||Li increased slowly from ≈62 to 142 mAh g^{-1} at a C/10 and then dropped rapidly to ≈52, 38, and 15 mAh g^{-1} when the C-rates were increased to C/5, C/2, and 1 C. The charge/discharge curves of LFP||UVp-Li and LFP||Li were also plotted (Figure 5e). At a current of C/10, LFP||UVp-Li delivered a discharge voltage of 3.38 V, which was close to the theoretical value of the LFP cathode (3.4 V vs Li^+/Li), and was higher than the LFP||Li (3.35 V). When the current density was increased to C/2 and 1C, the discharge voltage plateau of LFP||UVp-Li decreased slightly to ≈3.32 and ≈3.27 V, respectively. The midpoint discharge voltage of LFP||Li decreased to only 3.31 V when the current density was C/5. The discharge voltage could barely maintain a voltage plateau when further increased the C-rate to C/2 and 1C. The overpotential between the charge and discharge voltage of the LFP||Li was much higher than the LFP||UVp-Li at the same current density, indicating the benefits of using in situ polymerization and composited Li anode. Remarkably, LFP||UVp-Li retained as high as ≈84% capacity after 500 full cycles without any fluctuation (Figure 5f). In the same conditions, LFP||Li fluctuated seriously, and its capacity dropped to ≈49%. The initial coulombic efficiency (ICE) of LFP||UVp-Li was 95.2%, much higher than that of the LFP||Li (87.9%). The CE of LFP||UVp-Li was stable and an average CE of 99.84% was obtained after 500 cycles. For LFP||Li, the CE fluctuated largely during cycling despite the slightly higher average CE value (99.94%). The voltage profiles of LFP||UVp-Li overlapped well with the initial cycle (Figure 5g), further demonstrating its outstanding stability.

2.5. Versatility and Flexibility of UVp-Li-Based SSLMBs

It is recognized that increasing the areal capacity and operating voltage of the cathode is indispensable to achieving the high energy density of SSLMBs. UVp-Li is compatible with a wide range of high-capacity and high-voltage cathodes. An areal capacity of ≈0.5, 1.1, 2.0, and 2.9 mAh cm^{-2} can be obtained at 0.1 C when the loading mass of the LFP was increased from 4.2 to 19.4 mg cm^{-2} (**Figure 6**a), while the voltage hysteresis remained stable (Figure 6b). Besides, 4V-class LCO, NCM622, and NCA815 cathodes were also used for the in situ fabrication of SSLMBs with UVp-Li. The specific capacities could reach high values of ≈150, 164, and 174 mAh g^{-1} at 0.1 C for LCO||UVp-Li, NCM622||UVp-Li, and NCA815||UVp-Li, respectively (Figure 6c). No signs of cell failure or decomposition of the electrolyte were found when charging these batteries to a high voltage of 4.3 V. The cells could be readily cycled more than 50 times with high areal capacities at room temperature (Figure 6d). The ICE and CE were 92.8% and 99.2% for LCO||UVp-Li, 83.7% and 99.2% for NCM622||UVp-Li, and 78.4% and 99.1% for NCA815||UVp-Li, respectively. The CE values and cyclability can be further improved through surface modification or doping in future studies.

The intrinsic flexibility of the carbon fabric substrates endows good flexibility to the UVp-Li. A flexible pouch cell with an area of 10 cm^{-2} was assembled and tested to showcase the application of UVp-Li in the field of flexible SSLMBs. During more than 1000 times of dynamic bending, the high mass loading (LFP: 13 mg cm^{-2}) LFP||UVp-Li pouch cell was charged/discharged. The voltage plateau remained constant at ≈3.38 V, and the charge/discharge profiles overlapped well before bending (Figure 6e). The pouch cell could be cycled more than 100 times without cell failure (Figure S9, Supporting Information). The capacity decayed faster compared to the coin cell mainly due to the higher cycling areal capacity and lower operation pressure.[59,60] We demonstrated that a flexible LED panel could be lit on by the flexible pouch cell under different bending states (Figure 6f; and Video S1, Supporting Information). Moreover, it is also possible to assemble the pouch cell with the LCO cathode which delivered a higher operating voltage (Figure S10, Supporting Information). The pouch cell based on the SPE presented excellent safety performance and could consistently power on an LED even after harsh cutting tests (Figure S11, Supporting Information).

3. Conclusions

In conclusion, we have reported for the first time a UV-permeable and flexible Li metal anode, named UVp-Li. It enabled the

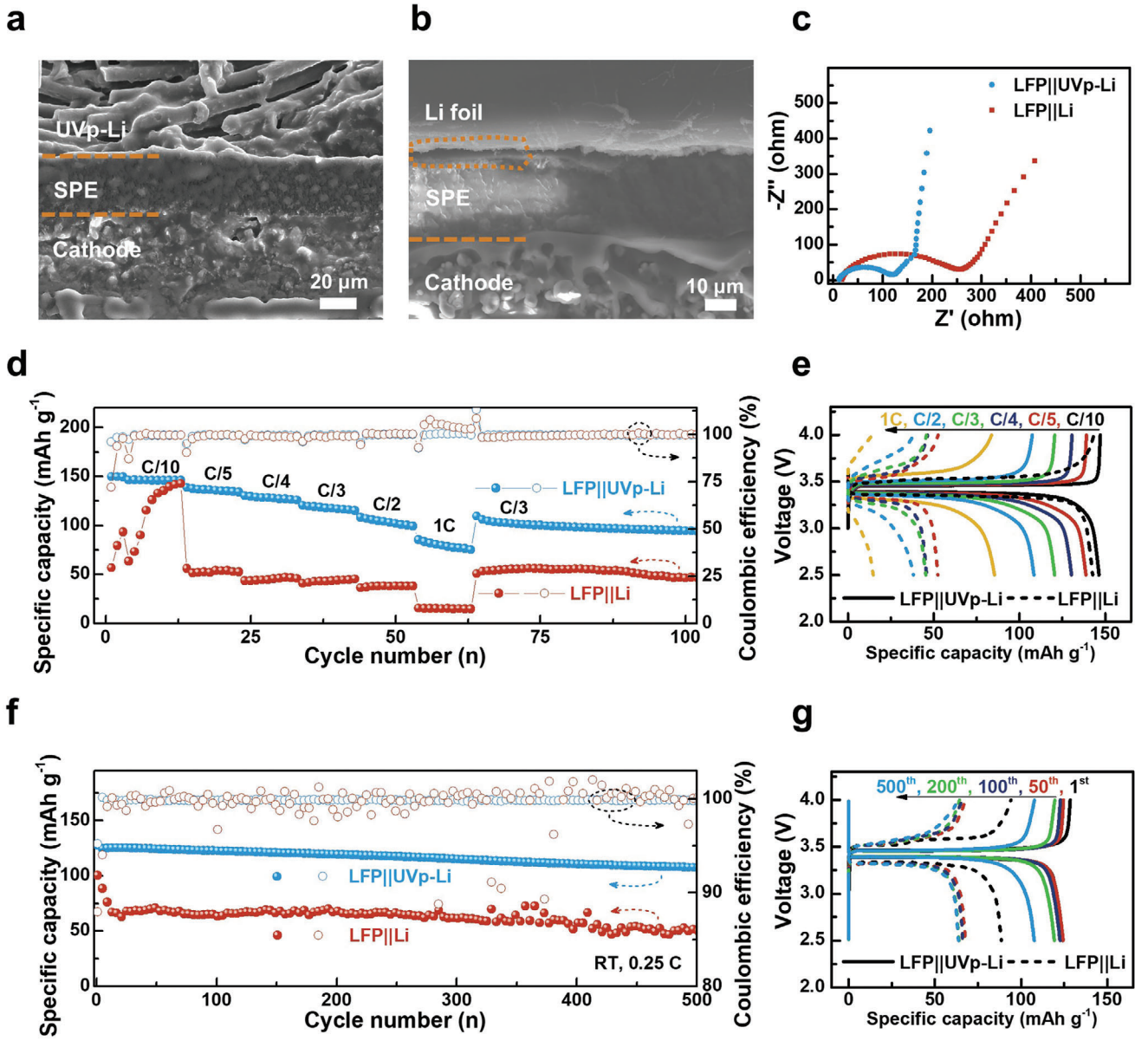

Figure 5. Comparison of the in situ fabricated LFP||UVp-Li and single side-cured LFP||Li full cells. Cross-sectional SEM images of, a) LFP||UVp-Li, and b) LFP||Li. c) EIS of uncycled LFP||UVp-Li and LFP||Li. d) Rate performances of the full cells. 1C was 0.85 mA cm^{-2} based on the mass of LFP. e) Voltage profiles of LFP||UVp-Li (solid lines) and LFP||Li (dashed lines) under rate performance test. f) Long-term cycling test of the full batteries. 1C was 0.65 mA cm^{-2} based on the mass of LFP. g) Voltage evolution of LFP||UVp-Li (solid lines) and LFP||Li (dashed lines).

fabrication of interface-gapless SSLMBs, via one-step in situ UV-induced curing of anode, SPE, and cathode. Conformal interfacial contact was achieved at both the anode|SPE site and the cathode|SPE site. As a result, the UVp-Li||UVp-Li symmetric cell showed stable, and low overpotential even under a high current of 1 mA cm^{-2} and long cycling stability of over 1000 h at room temperature. LFP||UVp-Li could sustain high charge/discharge rates up to 1C at room temperature and remained a high capacity retention of ≈84% after 500 cycles. UVp-Li was also compatible with various high-capacity and 4V-class cathodes for high-energy SSLMBs. Moreover, the pouch cell tests presented outstanding charge/discharge stability during 1000 cycles of dynamic bending. Since UV-induced in situ fabrication is a highly scalable process, we envision that UVp-Li can be integrated into the roll-to-roll fabrication process of high-performance SSLMBs in the near future.

4. Experimental Section

Materials: Succinonitrile, lithium bis(trifluoromethane sulfonyl)imide (LiTFSI), poly(ethylene glycol) diacrylate (DA700), and photoinitiator 1173 with the highest purity were purchased from Sigma-Aldrich without further treatment. Fluoroethylene carbonate (FEC) and lithium difluoro(oxalato)borate (LiDFOB)

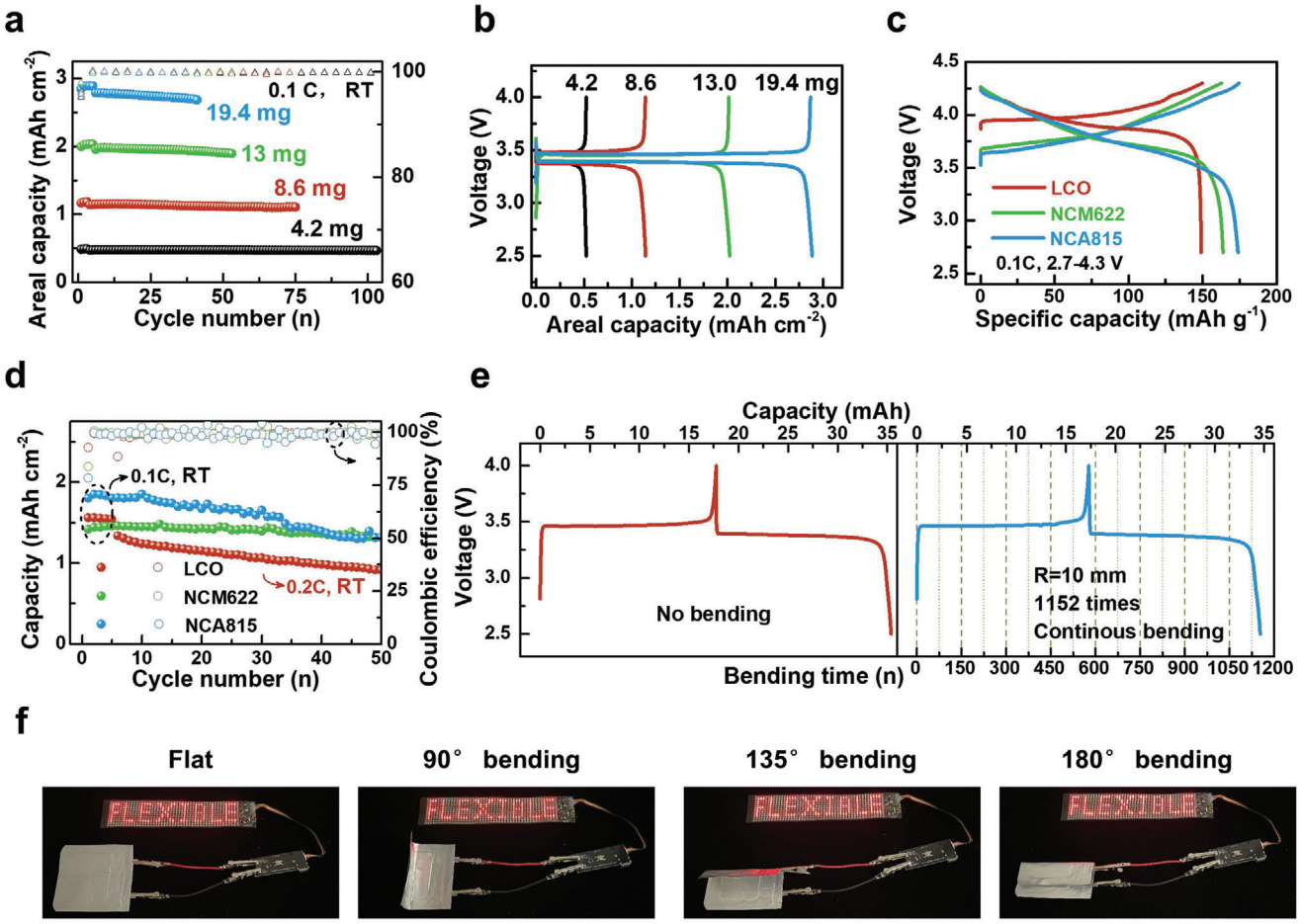

Figure 6. Demonstration of high-mass loading batteries, high-voltage batteries, and flexible pouch cells based on UVp-Li. a) Cycling performances, and b) the corresponding voltage profiles of the in situ fabricated LFP||UVp-Li with different mass loadings. c) Voltage profiles, and d) cycling stability of the high-voltage LCO||UVp-Li, NCM622||UVp-Li, and NCA815||UVp-Li cells. e) Voltage profiles of a 10 cm^2 high-loading LFP||UVp-Li flexible pouch cell under flat/dynamic bending states. The bending radius was 10 mm and 1152 bending times were applied each charge/discharge cycle during dynamic bending. f) Digital images showing the flexible battery can power the LED panel under various bending states.

were received from Shenzhen Capchem Technology as a kind donation. Other materials for the preparation of batteries were purchased from Shenzhen Kejing Star Technology Ltd. The carbon cloth (W0S1011) was purchased from CeTech, Taiwan. The copper-coated carbon cloth was prepared through a polymer-assisted metal deposition (PAMD) method as reported by the group.[61] The composited Li metal anode (UVp-Li) was prepared using the same method as the previously published work.[50] The mass of Li was carefully controlled to maintain the large pores for UV transmission.

Preparation of Electrolyte Precursor: The liquid electrolyte was prepared by firstly dissolving LiTFSI in succinonitrile at 50 °C with magnetic stirring (solution A). 5 wt% of FEC and 1 wt% LiDFOB were added into DA700 at 50 °C as additives (solution B). The liquid electrolyte precursor solution was prepared by direct mixing of the solutions A and B at 50 °C with 1173 as photoinitiator (1 wt% of DA700). The liquid precursor should be freshly prepared before use to avoid any self-polymerization.

Fabrication of the Freestanding SPE: The precursor solution was injected into a homemade mold made of two pieces of glass slides, and a 200 µm silicon framework was used to fix the thickness. The polymerization was carried out using a UV light (365 nm, with an intensity of ≈2 W cm^{-2}) at a distance of 10 cm for 5–10 min. A thin polyethylene-supported electrolyte was prepared by using the commercially available polyethylene (25 µm) as a supporting membrane.

Preparation of the Cathodes: The LFP cathodes with different loading masses were prepared through a conventional slurry-based method. The LFP powders, super P, and the polyvinylidene difluoride were ball-mixed with a suitable amount of *N*-Methylpyrrolidone and coated on precleaned Al foils followed by vacuum drying at 80 °C for 4 h and 12 °C for 8 h. High-loading LCO (10.5 mg cm^{-2}), NCM622 (8.8 mg cm^{-2}), NCA815 (10.6 mg cm^{-2}) were directly purchased from Shenzhen Kejing Star Technology Ltd.

Preparation of the Symmetric Cells, Full Batteries, and Pouch Cells: The in situ fabrication of the batteries was achieved by stacking the cathode/UVp-Li, polyethylene separator, and UVp-Li anode between two pieces of clean glass slides followed by infiltrating the precursor solution. After full infiltration of the solution

under a high vacuum for 30 min, UV irradiation was applied from the anode side for 5–10 min to complete the fabrication. The cells were then assembled into 2032-coin cells using stainless cases or pouch cells using Al laminated plastics. For the cells based on Li foil, the cathodes were cured with a polyethylene separator using UV-induced polymerization of liquid precursor first and assembled into cells with Li foil. The preparation of electrolyte precursor, SPE, and batteries was carried out in an Ar-filled glovebox with O_2 and H_2O content lower than 1 ppm.

Preparation of the Samples for Cross-Sectional Images: To acquire clear cross-sectional images of the batteries, the assembled cells were stacked together and fixed with scotch tapes before being mounted between two glass slides with two parts epoxies. The samples were then milled carefully using silicon carbide sandpapers from 60 to 2200 grit.

Characterization and Electrochemical Tests: The SEM images and optical images were obtained by FESEM (JSM6335F, JEOL, Japan) and Nikon Eclipse Ni-U, respectively. The UV transmittance was tested through a UV–Vis spectrometer (Cary 300, Varian, USA). A homemade electrochemical setup with a transparent glass cover was used for operando observation of the Li plating/stripping. CHI 660e was used for the test of ionic conductivity, EIS, CV, and LSV. The ionic conductivity (σ) of the SPE was tested by sandwiching the electrolyte between two pieces of stainless steel with a diameter of 16 mm and applying alternative current with a potential amplitude of 10 mV from the applied frequency of 10^5 Hz to 50 mHz. The ionic conductivity can be calculated from the equation

$$\sigma = \frac{d}{SR} \tag{1}$$

where d, S, and R are the thickness, area, and resistance of the SPE. The batteries were balanced for 60 min before the testing at different temperatures. The electrochemical voltage window was tested through LSV by using Li foil and stainless steel as electrodes in a coin cell at a scanning rate of 0.1 mV S^{-1} from 2 to 5 V. Cyclic voltammetry (CV) test was carried out at a scanning rate of 0.1 mV S^{-1} from 2 to −0.5 V to prove the stability of SPE at low voltage. EIS was carried out using similar parameters as the ionic conductivity with in situ and ex situ fabricated full cells. All the galvanostatic tests of the batteries were cycled on the Neware battery testing system (BTS-4008, Shenzhen, China) at 25 °C.

Supporting Information

Supporting Information is available from the Wiley Online Library or from the author.

Acknowledgements

The author would like to thank the financial support from the Research Grant Council (R5019-22F) and The Hong Kong Polytechnic University (U-ZEZ0).

Conflict of Interest

The authors declare no conflict of interest.

Data Availability Statement

The data that support the findings of this study are available in the Supporting Information of this article.

Keywords

flexible batteries, interfaces, lithium metal anodes, solid-state batteries, textile composite electrodes

Received: May 4, 2024
Revised: June 13, 2024
Published online: June 25, 2024

[1] J. Chang, Q. Huang, Y. Gao, Z. Zheng, *Adv. Mater.* **2021**, *33*, 2004419.
[2] C. Xie, Y. Guo, Z. Zheng, *CCS Chem* **2023**, *5*, 531.
[3] D. G. Mackanic, T. H. Chang, Z. Huang, Y. Cui, Z. Bao, *Chem. Soc. Rev.* **2020**, *49*, 4466.
[4] J. Chang, Q. Huang, Z. Zheng, *Joule* **2020**, *4*, 2208.
[5] X. Fan, C. Zhong, J. Liu, J. Ding, Y. Deng, X. Han, L. Zhang, W. Hu, D. P. Wilkinson, J. Zhang, *Chem. Rev.* **2022**, *122*, 17155.
[6] D. Zhou, D. Shanmukaraj, A. Tkacheva, M. Armand, G. Wang, *Chem* **2019**, *5*, 2326.
[7] X. Judez, G. G. Eshetu, C. Li, L. M. Rodriguez-Martinez, H. Zhang, M. Armand, *Joule* **2018**, *2*, 2208.
[8] J. Zheng, M. S. Kim, Z. Tu, S. Choudhury, T. Tang, L. A. Archer, *Chem. Soc. Rev.* **2020**, *49*, 2701.
[9] S. Nanda, A. Gupta, A. Manthiram, *Adv. Energy Mater.* **2020**, *11*, 2000804.
[10] M. Balaish, J. C. Gonzalez-Rosillo, K. J. Kim, Y. Zhu, Z. D. Hood, J. L. M. Rupp, *Nat. Energy* **2021**, *6*, 227.
[11] S. Li, S. Q. Zhang, L. Shen, Q. Liu, J. B. Ma, W. Lv, Y. B. He, Q. H. Yang, *Adv. Sci.* **2020**, *7*, 1903088.
[12] S. Xia, X. Wu, Z. Zhang, Y. Cui, W. Liu, *Chem* **2019**, *5*, 753.
[13] Z. Wang, L. Shen, S. Deng, P. Cui, X. Yao, *Adv. Mater.* **2021**, *33*, 2100353.
[14] J. Wu, S. Liu, F. Han, X. Yao, C. Wang, *Adv. Mater.* **2021**, *33*, 2000751.
[15] D. H. S. Tan, A. Banerjee, Z. Chen, Y. S. Meng, *Nat. Nanotechnol.* **2020**, *15*, 170.
[16] D. Cao, X. Sun, Q. Li, A. Natan, P. Xiang, H. Zhu, *Matter* **2020**, *3*, 57.
[17] X.-B. Cheng, C.-Z. Zhao, Y.-X. Yao, H. Liu, Q. Zhang, *Chem* **2019**, *5*, 74.
[18] J. Lee, S. H. Jeong, J. S. Nam, M. Sagong, J. Ahn, H. Lim, I. D. Kim, *EcoMat* **2023**, *5*, e12416.
[19] K. Shi, A. Dutta, Y. Hao, M. Zhu, L. He, Y. Pan, X. Xin, L.-F. Huang, X. Yao, J. Wu, *Adv. Funct. Mater.* **2022**, *32*, 2203652.
[20] D. Zhou, Y. B. He, R. Liu, M. Liu, H. Du, B. Li, Q. Cai, Q. H. Yang, F. Kang, *Adv. Energy Mater.* **2015**, *5*, 1500353.
[21] P. Jaumaux, Q. Liu, D. Zhou, X. Xu, T. Wang, Y. Wang, F. Kang, B. Li, G. Wang, *Angew. Chem. Int. Ed. Engl.* **2020**, *59*, 9134.
[22] Y. Yan, J. Ju, S. Dong, Y. Wang, L. Huang, L. Cui, F. Jiang, Q. Wang, Y. Zhang, G. Cui, *Adv. Sci.* **2021**, *8*, 2003887.
[23] F. Q. Liu, W. P. Wang, Y. X. Yin, S. F. Zhang, J. L. Shi, L. Wang, X. D. Zhang, Y. Zheng, J. J. Zhou, L. Li, Y. G. Guo, *Sci. Adv.* **2018**, *4*, eaat5383.
[24] Q. Zhao, X. Liu, S. Stalin, K. Khan, L. A. Archer, *Nat. Energy* **2019**, *4*, 365.
[25] V. Vijayakumar, B. Anothumakkool, S. Kurungot, M. Winter, J. R. Nair, *Energy Environ. Sci.* **2021**, *14*, 2708.
[26] C. Ma, W. Cui, X. Liu, Y. Ding, Y. Wang, *InfoMat* **2021**, *4*, e12232.
[27] G. Yang, W. Hou, Y. Zhai, Z. Chen, C. Liu, C. Ouyang, X. Liang, P. Paoprasert, N. Hu, S. Song, *EcoMat* **2023**, *5*, e12325.

[28] Q. Liu, B. Cai, S. Li, Q. Yu, F. Lv, F. Kang, Q. Wang, B. Li, *J. Mater. Chem. A.* **2020**, *8*, 7197.
[29] M. B. Effat, Z. Lu, A. Belotti, J. Yu, Y.-Q. Lyu, F. Ciucci, *J. Power Sources* **2019**, *436*, 226802.
[30] P. Li, S. Wang, J. Hao, X. Wang, S. M. Hao, Y. Lu, H. Li, W. Zhou, Y. Li, *Angew. Chem. Int. Ed. Engl.* **2023**, *62*, e202309613.
[31] M. Chen, M. Zhong, J. A. Johnson, *Chem. Rev.* **2016**, *116*, 10167.
[32] X. Pan, M. A. Tasdelen, J. Laun, T. Junkers, Y. Yagci, K. Matyjaszewski, *Prog. Polym. Sci.* **2016**, *62*, 73.
[33] C. Mendes-Felipe, J. Oliveira, I. Etxebarria, J. L. Vilas-Vilela, S. Lanceros-Mendez, *Adv. Mater. Technol.* **2019**, *4*, 1800618.
[34] S. Qi, S. Li, W. Zou, W. Zhang, X. Wang, L. Du, S. Liu, J. Zhao, *Small* **2022**, *18*, e2202013.
[35] S. Oh, V. H. Nguyen, V. T. Bui, S. Nam, M. Mahato, I. K. Oh, *ACS Appl. Mater. Interfaces* **2020**, *12*, 11657.
[36] K. Zhang, F. Wu, X. Wang, S. Weng, X. Yang, H. Zhao, R. Guo, Y. Sun, W. Zhao, T. Song, X. Wang, Y. Bai, C. Wu, *Adv. Energy Mater.* **2022**, *12*, 2200368.
[37] B. Yuan, B. Zhao, Q. Wang, Y. Bai, Z. Cheng, Z. Cong, Y. Lu, F. Ji, F. Shen, P.-F. Wang, X. Han, *Energy Storage Mater.* **2022**, *47*, 288.
[38] X. Chen, W. He, L.-X. Ding, S. Wang, H. Wang, *Energy Environ. Sci.* **2019**, *12*, 938.
[39] Q. Pang, L. Zhou, L. F. Nazar, *Proc. Natl. Acad. Sci. USA* **2018**, *115*, 12389.
[40] L. Chen, Y. Li, S.-P. Li, L.-Z. Fan, C.-W. Nan, J. B. Goodenough, *Nano Energy* **2018**, *46*, 176.
[41] Y. Xiao, K. Turcheniuk, A. Narla, A. Y. Song, X. Ren, A. Magasinski, A. Jain, S. Huang, H. Lee, G. Yushin, *Nat. Mater.* **2021**, *20*, 984.
[42] H. Zhang, X. An, Y. Yang, Y. Long, S. Nie, L. Liu, G. Yang, Z. Tian, H. Cao, Z. Cheng, H. Liu, Y. Ni, *EcoMat* **2022**, *5*, e12317.
[43] C. M. Costa, R. Gonçalves, S. Lanceros-Méndez, *Energy Storage Mater.* **2020**, *28*, 216.
[44] P. Leung, J. Bu, P. Quijano Velasco, M. R. Roberts, N. Grobert, P. S. Grant, *Adv. Energy Mater.* **2019**, *9*, 1901418.
[45] F. Zhou, Z. Li, Y. Y. Lu, B. Shen, Y. Guan, X. X. Wang, Y. C. Yin, B. S. Zhu, L. L. Lu, Y. Ni, Y. Cui, H. B. Yao, S. H. Yu, *Nat. Commun.* **2019**, *10*, 2482.
[46] W. Liu, C. Yi, L. Li, S. Liu, Q. Gui, D. Ba, Y. Li, D. Peng, J. Liu, *Angew. Chem. Int. Ed. Engl.* **2021**, *60*, 12931.
[47] X. Xing, Y. Li, S. Wang, H. Liu, Z. Wu, S. Yu, J. Holoubek, H. Zhou, P. Liu, *ACS Energy Lett.* **2021**, *6*, 1831.
[48] Y. Yang, H. Chen, J. Wan, R. Xu, P. Zhang, W. Zhang, S. T. Oyakhire, S. C. Kim, D. T. Boyle, Y. Peng, Y. Ma, Y. Cui, *Adv. Energy Mater.* **2022**, *12*, 2201160.
[49] Y. Liu, D. Lin, Y. Jin, K. Liu, X. Tao, Q. Zhang, X. Zhang, Y. Cui, *Sci. Adv.* **2017**, *3*, eaao0713.
[50] J. Chang, H. Hu, J. Shang, R. Fang, D. Shou, C. Xie, Y. Gao, Y. Yang, Q. N. Zhuang, X. Lu, Y. K. Zhang, F. Li, Z. Zheng, *Small* **2022**, *18*, e2105308.
[51] L. Wang, J. Shang, Q. Huang, H. Hu, Y. Zhang, C. Xie, Y. Luo, Y. Gao, H. Wang, Z. Zheng, *Adv. Mater.* **2021**, *33*, 2102802.
[52] R. Lin, Y. He, C. Wang, P. Zou, E. Hu, X. Q. Yang, K. Xu, H. L. Xin, *Nat. Nanotechnol.* **2022**, *17*, 768.
[53] Z. Hu, F. Xian, Z. Guo, C. Lu, X. Du, X. Cheng, S. Zhang, S. Dong, G. Cui, L. Chen, *Chem. Mater.* **2020**, *32*, 3405.
[54] H.-S. Shin, W. Jeong, M.-H. Ryu, S. W. Lee, K.-N. Jung, J.-W. Lee, *Chem. Eng. J.* **2022**, *433*, 133753.
[55] A. Wang, S. Geng, Z. Zhao, Z. Hu, J. Luo, *Adv. Funct. Mater.* **2022**, *32*, 2201861.
[56] D. Li, C. Xie, Y. Gao, H. Hu, L. Wang, Z. Zheng, *Adv. Energy Mater.* **2022**, *12*, 2200584.
[57] J. Cai, L. Wang, Q. Huang, W. Yu, C. Xie, Z. Zheng, *Adv. Energy Mater.* **2023**, *14*, 2303088.
[58] J. P. Wang, F. Lang, Q. Li, *EcoMat* **2023**, *5*, e12354.
[59] S. Jiao, J. Zheng, Q. Li, X. Li, M. H. Engelhard, R. Cao, J.-G. Zhang, W. Xu, *Joule* **2018**, *2*, 110.
[60] C. Fang, B. Lu, G. Pawar, M. Zhang, D. Cheng, S. Chen, M. Ceja, J.-M. Doux, H. Musrock, M. Cai, *Nat. Energy* **2021**, *6*, 987.
[61] J. Chang, J. Shang, Y. Sun, L. K. Ono, D. Wang, Z. Ma, Q. Huang, D. Chen, G. Liu, Y. Cui, Y. Qi, Z. Zheng, *Nat. Commun.* **2018**, *9*, 4480.